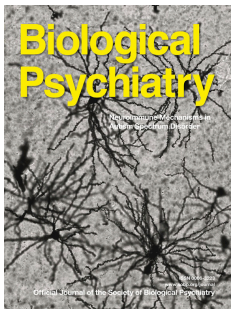
# Journal Pre-proof




Brain NaV1.5 fine-tunes neuronal excitability to facilitate female-directed social behavior in male mice

Wei Ke, Heyuan Zhang, Liang Li, Yujie Xiao, Shuxuan Lyu, Quansheng He, Xiaoxue Zhang, Luping Yin, Yilin Tai, Yousheng Shu

PII: S0006-3223(26)01611-2

DOI: https://doi.org/10.1016/j.biopsych.2026.10.008

Reference: BPS 16251

To appear in: *Biological Psychiatry*

Received Date: 22 January 2026

Revised Date: 10 September 2026

Accepted Date: 10 October 2026

Please cite this article as: Ke W., Zhang H., Li L., Xiao Y., Lyu S., He Q., Zhang X., Yin L., Tai Y. & Shu Y., Brain NaV1.5 fine-tunes neuronal excitability to facilitate female-directed social behavior in male mice, *Biological Psychiatry* (2026), doi: https://doi.org/10.1016/j.biopsych.2026.10.008.

This is a PDF of an article that has undergone enhancements after acceptance, such as the addition of a cover page and metadata, and formatting for readability. This version will undergo additional copyediting, typesetting and review before it is published in its final form. As such, this version is no longer the Accepted Manuscript, but it is not yet the definitive Version of Record; we are providing this early version to give early visibility of the article. Please note that Elsevier's sharing policy for the Published Journal Article applies to this version, see: https://www.elsevier.com/about/policies-and-standards/sharing#4-published-journal-article. Please also note that, during the production process, errors may be discovered which could affect the content, and all legal disclaimers that apply to the journal pertain.

© 2026 Published by Elsevier Inc on behalf of Society of Biological Psychiatry.

Journal Pre-proof

# Brain $Na_V1.5$ fine-tunes neuronal excitability to facilitate female-directed social behavior in male mice

Wei Ke[1], Heyuan Zhang[1], Liang Li[1], Yujie Xiao[2], Shuxuan Lyu[1], Quansheng He[1], Xiaoxue Zhang[1], Luping Yin[3], Yilin Tai[4], Yousheng Shu[1]*

[1] Department of Neurology, Jinshan Hospital, Institute for Translational Brain Research, Fudan SANS Neuroscience Center, State Key Laboratory of Brain Function and Disorders, MOE Frontiers Center for Brain Science, Fudan University, Shanghai 201508, China.

[2] College of Elementary Education, Capital Normal University, Beijing 100048, China.

[3] Westlake Laboratory of Life Sciences and Biomedicine, School of Life Sciences, Westlake University, Institute of Biology, Westlake Institute for Advanced Study, Hangzhou 310024, China.

[4] State Key Laboratory of Brain Function and Disorders and MOE Frontiers Center for Brain Science, and the Institutes of Brain Science, Fudan University, Shanghai 200032, China.

* Corresponding author: Yousheng Shu, yousheng@fudan.edu.cn

Running title: Brain $Na_V1.5$ regulates male social behavior

Journal Pre-proof

## Abstract

**Background:** The voltage-gated sodium channel $Na_V1.5$, an essential subtype for cardiac action potential generation, is also enriched in limbic regions of the brain, but its function in the central nervous system remains poorly understood.

**Methods:** We performed RNAscope, immunostaining, electrophysiology, fiber photometry, *Scn5a* knockdown, and behavioral testing to dissect the functional role of $Na_V1.5$ in the brain.

**Results:** $Na_V1.5$ channels are enriched in neurons of posterior bed nucleus of the stria terminalis (BNSTp) and accumulated at the axon initial segment. Activation of these tetrodotoxin-resistant channels lowers action potential threshold and accelerates spike initiation at relatively hyperpolarized levels of membrane potential ($V_m$). *In vivo* fiber photometry showed that BNSTp $Na_V1.5$-expressing neurons in male mice were recruited by salient social stimuli and exhibited hyperpolarizing $V_m$ dynamics during social contacts. *Scn5a* knockdown selectively attenuated neuronal responses to female chemosensory cues, and disrupted sex preference and female-directed behaviors.

**Conclusions:** These findings identify $Na_V1.5$ as a $V_m$ state-dependent regulator of BNSTp neuronal excitability, and reveal an unexpected role of this channel subtype in female-cue processing and female-directed social behavior in males.


**Keywords**: $Na_V1.5$; BNSTp; neuronal excitability; social-cue processing; sex preference; social behaviors.

Journal Pre-proof

## Introduction

Social behaviors such as mating, aggression, and parental care are driven by conspecific sensory cues that are primarily processed through a conserved vomeronasal pathway in rodents(1,2). Sex-specific pheromonal signals sensed by the vomeronasal organ (VNO) are transmitted via the accessory olfactory bulb (AOB) to limbic nodes including the medial amygdala (MeA) and the principal subdivision of the bed nucleus of the stria terminalis (BNSTpr). These signals are subsequently relayed to hypothalamic regions such as the medial preoptic area (MPOA), ventrolateral ventromedial hypothalamus (VMHvl), and ventral premammillary nucleus (PMv), coordinating sex-specific motivational states and behavioral outputs(3–7).

Neuronal populations in these regions encode sex-specific social cues in distinct sex-biased patterns(8). While VMHvl and PMv cell populations are biased toward male cues, certain types of BNSTpr neurons preferentially respond to female intruders(5,9,10). These sex-biased representations are highly plastic and are shaped dynamically by experience, internal states and environmental context(11–13). Social and sexual experiences sharpen the signal-to-noise ratio for sex-specific encoding, facilitating transitions from investigation to consummatory behaviors(10,14). In addition, the tuning properties can also be reshaped by upstream inputs. Silencing BNSTpr Esr1$^{+}$ (estrogen receptor alpha) neurons in male mice reverses the typical male-biased coding in VMHvl to a female-dominant pattern, markedly suppressing aggression(5). These findings highlight that sex-specific neural representations are essential for appropriate social behavior.

*In vivo* imaging from posterior BNST (BNSTp) subdivisions found that the number of female-responsive cells is approximately twofold that of male-responsive ones(5), explaining female-biased coding observed in bulk calcium imaging. However, the mechanism that establish this bias remain unclear. One

possibility is a hardwired, labeled-line circuit architecture(1,7,15), in which the overrepresented population receives stronger or more numerous upstream inputs. Alternatively, differences in intrinsic excitability among BNSTp subpopulations could set recruitment thresholds, thereby determining the size of the neuronal ensembles engaged by a given sex-specific cue.

Voltage-gated sodium channels ($Na_V$) play crucial roles in regulating neuronal excitability and firing patterns(16), with a cell type or brain region-specific expression pattern. Intriguingly, $Na_V1.5$, encoded by *Scn5a* and responsible for cardiomyocyte excitability(17), is also highly enriched in the BNSTp and other limbic regions associated with social behaviors(18,19), but its function in the brain remains largely unexplored. Its pronounced steady-state inactivation at resting or depolarized membrane potentials ($V_m$) suggests that $Na_V1.5$ may act as a $V_m$ state-dependent regulator of BNSTp neuronal responsiveness.

In this study, we identify $Na_V1.5$ as a state-dependent excitability regulator in the BNSTp. $Na_V1.5$ is enriched in BNSTp neurons, including PMv-projecting neurons, and accumulates at the axon initial segment (AIS), where it lowers action potential (AP) threshold and accelerates AP initiation under relatively hyperpolarized membrane-potential states. *In vivo* calcium photometry revealed that $Na_V1.5$-expressing BNSTp neurons are broadly recruited by salient social stimuli, including conspecific and pup-related cues. Voltage photometry further showed that BNSTp $Na_V1.5^+$ neurons exhibit social behavior-associated hyperpolarizing voltage dynamics that may favor $Na_V1.5$ availability. *Scn5a* knockdown (KD) selectively attenuated neuronal responses evoked by female cues and disrupted sex preference and female-directed behaviors. Together, our findings support a model in which $Na_V1.5$ fine-tunes BNSTp excitability during social-cue processing and facilitates female-directed social behavior in males.

## Methods and Materials

### Animals

All animal procedures were approved by the Animal Care and Use Committee of Fudan University (2021JS-ITBR-001) and conducted according to institutional and national guidelines. Wild-type C57BL/6J mice were obtained from GemPharmatech (N000295), and $Na_V1.5$-cre mice were custom-generated by GemPharmatech. Mice were group-housed under a 12 h light/dark cycle with *ad libitum* food and water. Male mice were used unless otherwise specified. Female mice used for female BNSTp photometry were ovariectomized (OVX), and sexually receptive females used in mating assays were OVX and hormone-primed before testing as described previously (20).

### Electrophysiological recording

Mice were anesthetized with pentobarbital (100 mg/kg, i.p.), then perfused transcardially with ice-cold sucrose-based cutting solution, and 200-μm coronal slices were prepared in this solution. Slices were recovered in oxygenated ACSF (in mM): 126 NaCl, 2.5 KCl, 1.25 $NaH_2PO_4$, 26 $NaHCO_3$, 25 glucose, 2 $MgSO_4$, 2 $CaCl_2$ (315 mOsm, pH 7.4) at ~34.5°C for 40-50 min and recorded at room temperature. Current-clamp recordings from BNSTp neurons were achieved using an internal solution containing (in mM): 140 K-gluconate, 3 KCl, 2 $MgCl_2$, 10 HEPES, 0.2 EGTA, 2 $Na_2ATP$, and 0.2% biocytin (280–290 mOsm, pH 7.2–7.3). The first AP in trains fired at ~20 Hz was chosen for analysis. The AP threshold was defined at *dV/dt* = 20 V/s, and AP amplitude, half-width, and maximal/minimal dV/dt were quantified from the same AP waveforms. $Na^+$ current recording were obtained from somata, somatic nucleated patches, and axon blebs using a Cs-based internal solution (in mM): 125 CsCl, 10 NaCl, 2 $MgCl_2$, 0.5 $CaCl_2$, 2 $Na_2ATP$, 0.5 $Na_3GTP$, 10 HEPES, 10 EGTA, and 2 TEA (290 mOsm, pH 7.3). TTX-resistant currents were isolated in the presence of TTX (1 μM) and $Ca^{2+}$/$K^+$ channel blockers. QX-314 (0.5 mM) was used to

examine the contribution of $Na_V1.5$. Data were sampled at 25 kHz for current clamp and 50 kHz for voltage clamp; cells with series resistance >25 MΩ or >20% change were excluded. For knockdown experiments, PMv-projecting BNSTp neurons were recorded 3 weeks after injection of retrobeads to PMv and scramble or *Scn5a* shRNA viruses to BNSTp. Axon-bleb recordings were achieved from GFP-positive axon blebs 2-3 weeks after BNSTp AAV-DIO-EGFP injection in $Na_V1.5$-cre mice.

**Viral tools and stereotaxic surgery**

*Scn5a* shRNA (GCCGACAAGATGTTCACCTAT; Gene ID: 110876) was cloned into pAKD-CMV-bGlobin-eGFP-H1-shRNA (5.86 x 10^12 vg/mL; OBIO); scramble shRNA (TTCTCCGAACGTGTCACGT; 9.33 x 10^12 vg/mL; OBIO) served as control. Male C57BL/6J mice aged 6-8 weeks received bilateral BNSTp injections (coordinates AP/ML/DV: +0.14, ±0.75, -4.20 mm; 300 nL/site). Knockdown was assessed by $Na_V1.5$ immunoreactivity after 3 weeks and at 8 and 12 days for early-baseline validation. Retrobeads were injected into VTA (-3.27, ±0.25, -4.50 mm), PAG (-4.35, ±0.40, -2.80 mm), or PMv (-2.07, ±0.50, -5.50 mm) with a total volume of 100-150 nL per target region.

**Immunostaining and RNAscope**

For $Na_V1.5$ immunostaining, mice were transcardially perfused with saline followed by weak fixative (0.5% PFA)(21). Brains were post-fixed, cryoprotected, sectioned at 20 µm, and stained with $Na_V1.5$/AnkG antibodies. For retrobead co-labeling with *Scn5a*, antigen retrieval was omitted and protease treatment shortened to 15 min. For *cFos*/*Scn5a* RNAscope, male mice were exposed to female urine, male urine, or saline. A cotton swab loaded with 300 µL fresh urine or saline was touched to the nose five times and placed in the home cage for 10 min. Mice were perfused within 30 min after exposure to these stimuli. *cFos*-positive BNSTp neurons and *Scn5a* puncta were quantified with CellProfiler(22).

**Behavior tests**

For urine preference, mice were habituated for 15 min in a 40 × 40 × 40 cm arena and then allowed to explore two Petri dishes containing 20 μL male or female urine for 5 min. Investigation duration, latency, and entries were scored with EthoVision XT and manually validated. Preference index was calculated as (female − male)/(female + male) using duration or entry frequency. For chemogenetic activation, $Na_V1.5$-cre mice expressing BNSTp cre-dependent hM3Dq or mCherry were tested after saline or DCZ injection (0.1 mg/kg, i.p.). For habituation-dishabituation, mice received three 2-min presentations each of water, male urine, and female urine, with a reversed sequence used to control for novelty effects. For social interaction, mice were exposed to male or female intruders for 5 min, and behaviors were manually annotated from top-view videos using MATLAB(20,23).

**Fiber photometry**

For calcium photometry, AAV-DIO-NES-jRGECO1a was injected bilaterally into the BNSTp of $Na_V1.5$-cre mice. After 3 weeks, *Scn5a* shRNA or control virus was injected into the same region, followed by optical fiber implantation. Recordings included baseline acquisition and free interaction with adult male or female mice, male or female urine, pups, or a novel object. jRGECO1a fluorescence was synchronized with behavior video. For projection-specific photometry, retro-cre was injected into the PMv and cre-dependent jRGECO1a into the BNSTp. For voltage photometry, ASAP5 was expressed in BNSTp $Na_V1.5^+$ neurons, validated in slices by simultaneous whole-cell recording and high-speed imaging (1000 Hz), and recorded in freely moving mice during social interaction. For *Scn5a*-KD photometry, the same cohort was recorded at 3–8 days and 3 weeks after shRNA injection. Viral expression and fiber placement were verified histologically, and anterior BNST placements were excluded. Fluorescence signals were corrected for baseline drift before ΔF/F calculation.

**snRNA-seq and statistics**

Published mouse BNST snRNA-seq data (GSE126836)(24), including 76,693 neurons from 7 adult female and 8 adult male biological replicates, were reanalyzed using Seurat and LIGER annotations. Neuronal subtype annotations were imported from the LIGER object available on the Single Cell Portal. Neurons with normalized *Scn5a* expression >0.5 were classified as *Scn5a*$^{+}$. Data were analyzed using MATLAB and R. Shapiro-Wilk tests were applied to assess normality; paired or unpaired t-tests, Wilcoxon rank-sum tests, one-way ANOVA, or two-way ANOVA were used for comparisons. Significance was set at $p < 0.05$. Data are shown as mean ± SEM unless otherwise specified.

## Results

### Projection-specific distribution of *Scn5a* in BNST neurons

Previous studies revealed the presence of *Scn5a* mRNA in the central nervous system (CNS) including the BNST(18,19). To validate these findings, we performed RNAscope *in situ* hybridization using *Scn5a* probes (see Methods). Strong fluorescent *Scn5a* signals were detected in subdivisions of both anterior and posterior BNST (BNSTa and BNSTp, **Figures 1A** and **1B**), as well as brain regions implicated in social behaviors, including MeA, MPOA and VMH (**Figure S1A**).

Single-nuclei RNA-seq (snRNA-seq) analysis confirmed that *Scn5a* was expressed across multiple GABAergic BNST clusters, with a higher proportion of *Scn5a*$^{+}$ neurons in BNSTp than BNSTa (40.6% vs. 28.0%; **Figure 1C**). Within BNSTp, *Scn5a* broadly overlapped with known social behavior-related markers, including aromatase (Aro), Esr1, Esr2, Ar, Tac1, and Tac2 (**Figures 1D** and **S1B**). Despite the presence of sex-biased transcriptional signatures across BNSTp cell clusters(25), *Scn5a* mRNA levels were comparable between males and females (**Figures S1C-S1D**).

Given the absence of cluster-specific selectivity in *Scn5a* expression, we next investigated whether it is enriched within projection-defined neuronal

populations. We injected retrobeads into output targets of BNST(6,26,27), including PMv, midbrain ventral tegmental area (VTA) and periaqueductal gray (PAG) that was extensively innervated by BNST axons (**Figure S1E**), followed by RNAscope to assess *Scn5a* expression in retrogradely labeled BNST neurons (**Figures 1E-1H**). Strikingly, PMv-projecting neurons were located exclusively in the BNSTp, and most of them (~93.7%) expressed *Scn5a* (**Figures 1F-1H**). In contrast, VTA-projecting neurons, which mainly resided in the BNSTa, exhibited a smaller proportion of *Scn5a*$^+$ cells (~52.8%) (**Figures 1G-1H**). PAG-projecting neurons, which span both anterior and posterior subdivisions of BNST, displayed varying density of *Scn5a*$^+$ cells depending on their spatial locations (**Figures 1G-1H**). Together, these findings demonstrate that *Scn5a* expression in the BNST is enriched in the BNSTp and is particularly prominent in neurons projecting to the PMv, suggesting a functional specialization of $Na_V1.5$ in social behavior circuits.

**$Na_V1.5$ accumulates at the AIS and mediates TTX-resistant current**

$Na_V$ channels exhibit precise subcellular localization where they play distinct physiological roles(21,28). Immunostaining in BNST revealed strong $Na_V1.5$ immunosignals at the AIS, co-localizing with the AIS marker, ankyrin-G (AnkG) (**Figure 2A**). Similar to other neurons that typically express multiple $Na_V$ isoforms to support neuronal spiking activity(21,29), BNST neurons also expressed *Scn1a*, *Scn2a*, *Scn3a*, *Scn8a*, and *Scn9a* in addition to *Scn5a*, as revealed by ScRNA-seq data analysis (**Figure S1F**). To determine the functional contribution of $Na_V1.5$ to the total $Na^+$ currents, we performed whole-cell voltage-clamp recordings in BNST neurons. Distinct from most $Na_V$ isoforms in the brain, $Na_V1.5$ is resistant to micromolar concentrations of tetrodotoxin (TTX)(30), allowing pharmacological isolation of $Na_V1.5$ currents. The mean peak amplitude of total inward $Na^+$ currents was 4.45 ± 0.16 nA . Bath application of 1 μM TTX blocked most of the $Na^+$ currents but revealed a residual inward current, with an average amplitude of 0.49 ± 0.03 nA,

corresponding to ~11.0% of the total $Na^+$ currents (**Figures 2B-2C**). This TTX-resistant current was abolished by subsequent bath application of 0.5 mM QX-314, a concentration capable of blocking $Na_V1.5$(31) (**Figures 2D-2E**).

TTX-resistant $Na^+$ currents were detected in whole-cell somatic recordings but not in somatic nucleated patches (**Figure 2F**), consistent with the AIS enrichment of $Na_V1.5$. Direct axon-bleb recordings(21,32) confirmed TTX-resistant $Na^+$ currents at the AIS and revealed the voltage dependence of activation ($V_{1/2}$ = –24.9 ± 3.7 mV) and steady-state inactivation ($V_{1/2}$ = –86.5 ± 2.7 mV; **Figures 2G-2I**), consistent with previously reported gating properties of $Na_V1.5$ in culture systems(33). These results suggest that the availability of $Na_V1.5$ channels is strongly voltage dependent and these channels are largely inactivated at the resting $V_m$.

**$Na_V1.5$ enhances neuronal responsiveness at hyperpolarized $V_m$**

The enrichment of $Na_V1.5$ at the AIS suggests a role of this channel in modulating neuronal excitability. To test this, we performed whole-cell current-clamp recordings from randomly selected BNSTp neurons in acute slices, with their $V_m$ held at about –65 mV. The presence of $Na_V1.5$ in recorded neurons was confirmed by *post hoc* avidin-biocytin staining combined with immunostaining (**Figure 3A**). Based on the presence or absence of $Na_V1.5$ immunofluorescence at the AnkG-labeled AIS, neurons were classified as $Na_V1.5^+$ or $Na_V1.5^-$. $Na_V1.5$ immunosignals at the AIS of $Na_V1.5^+$ neurons, peaked at approximately 12 μm from the soma and were significantly stronger than those of $Na_V1.5^-$ neurons (**Figure 3B**). Current-clamp recordings revealed that $Na_V1.5^+$ neurons had more hyperpolarized AP thresholds, higher AP amplitudes, and faster AP upstroke kinetics than $Na_V1.5^-$ neurons (**Figures 3C -3D**).

To establish a causal role of $Na_V1.5$ in regulating neuronal excitability, we achieved *Scn5a* knockdown (KD) through injecting an adeno-associated virus

(AAV) carrying shRNA targeting *Scn5a* to the BNSTp. Three weeks after virus injection, we performed immunostaining and confirmed an effective downregulation of $Na_V1.5$ expression (**Figures 3E-3F**). Retrogradely labeled PMv-projecting neurons exhibited a dramatic reduction in the TTX-resistant currents in KD mice (56.3 ± 5.7 pA, n = 39 cells), compared to control mice injected with viruses carrying scramble shRNA (339 ± 26 pA, n = 52 cells; **Figure 3G**), further validating a high KD efficiency.

We next recorded from virally infected PMv-projecting neurons to assess the functional consequences of *Scn5a* KD (**Figure S2A**). Given that $Na_V1.5$ channels are largely inactivated near the resting $V_m$ (–51.0 ± 1.3 mV), we hyperpolarized the recorded cells to approximately –65 mV to increase the availability of $Na_V1.5$ channels (**Figure S2B**). At this relatively hyperpolarized $V_m$ level, the overall spiking frequency of *Scn5a*-KD neurons examined by 500-ms step current injections showed no significant difference from control cells (**Figures 3H** and **S2C**). However, close examination of the initial AP (**Figures 3I**) revealed that, similar to $Na_V1.5^-$ neurons, *Scn5a*-KD neurons exhibited depolarized AP thresholds and reduced AP amplitudes as compared to control cells (**Figures 3J-3K**). Furthermore, *Scn5a* KD significantly delayed the onset of the first AP in response to step current injection (**Figure 3L**), an effect most pronounced with weak current injections (**Figures S2D-S2E**). All these differences between control and KD neurons were abolished when neurons were recorded at the depolarized resting $V_m$, where $Na_V1.5$ is mostly inactivated (**Figures 3I-3L** and **S2F**). These results reveal a $V_m$-dependent role of $Na_V1.5$ in enhancing excitability and accelerating AP initiation of PMv-projecting BNSTp neurons.

### *Scn5a* knockdown in male BNSTp disrupts sex preference

Given the role of $Na_V1.5$ in enhancing BNSTp neuronal responsiveness and the established involvement of BNSTp in sex preference and social behavior[5,8,9,34,35], we tested whether BNSTp *Scn5a* KD alters male social

behavior. In the urine preference assay, control males preferred female urine, whereas *Scn5a*-KD males lost this preference, as reflected by a reduced preference index despite unchanged exploration frequency (**Figures 4A-4C**). In an olfactory habituation/dishabituation assay(36,37), both groups habituated to repeated male urine and dishabituated upon first exposure to female urine, indicating intact urinary sex-cue discrimination (**Figures 4D-4E** and **S3A-S3B**).

We next assessed social interaction with male and female intruders. Control males showed a strong preference for female intruders, with longer and more frequent bouts of anogenital sniffing, body investigation, and attempts to mount (**Figure 4F**). In contrast, *Scn5a*-KD males showed reduced female-directed social behaviors without changes in locomotor activity or anxiety-like behavior (**Figures 4F-4G**); total interaction time and mean bout duration with female intruders were reduced to levels comparable to those with male intruders, and mounting attempts were significantly decreased (**Figures 4H-4J** and **S3C**). Chemogenetic activation of hM3Dq-expressing BNSTp $Na_V1.5^+$ neurons did not alter female urine investigation compared with saline treatment or mCherry controls (**Figure S3D**), indicating that this population is not a simple command ensemble sufficient to impose female cue preference.

To determine whether this behavioral specificity reflected female-cue specific *Scn5a* expression, we performed *cFos/Scn5a* codetection after urine exposure. Both male and female urine exposures recruited BNSTp *cFos*$^+$ neurons, most urine-responsive *cFos*$^+$ neurons expressed *Scn5a*, and neither *cFos*$^+$ neuron recruitment nor *Scn5a* expression within *cFos*$^+$ neurons differed between female and male-urine conditions (**Figures S3E-S3I**). Together, these results indicate that *Scn5a* KD disrupts female-directed behavioral responses without impairing urinary sex discrimination, likely by reducing $Na_V1.5$-dependent excitability in broad BNSTp circuits rather than a specific female-cue-responsive population.

**$Na_V1.5$ shapes BNSTp population activity evoked by social cues**

To determine how *Scn5a* KD alters social-cue-evoked activity, we performed *in vivo* fiber photometry from BNSTp $Na_V1.5^+$ neurons in freely behaving $Na_V1.5$-cre mice. Cre-dependent jRGECO1a was expressed in the BNSTp, followed 3 weeks later by *Scn5a* shRNA or scramble virus injection and optical fiber implantation (**Figures 5A-5B**).

In control males, calcium responses of BNSTp $Na_V1.5^+$ neurons to female intruders and female urine were stable across pre- and post-recording sessions (**Figures 5C**). During free social interaction, calcium transients peaked at first contact and declined across subsequent investigation bouts (**Figures 5D-5F**). These neurons showed weaker responses during intromission but detectable activation at ejaculation (**Figures S4A-S4C**), indicating recruitment during later mating phases. Across stimulus types, BNSTp $Na_V1.5^+$ neurons responded to salient social cues, including intruders, urine, and pups, but minimally to an object (**Figures 5G-5I**). Pup-evoked responses were comparable to female-evoked responses, supporting a broader role in salient social-cue processing rather than exclusive encoding of opposite-sex cues. Our projection-specific recordings further showed that PMv-targeting BNSTp neurons were recruited by intruder and urine stimuli (**Figures S4D-S4G**).

Because the availability of $Na_V1.5$ channels depends on relatively hyperpolarized $V_m$ that allow their recovery from inactivation (**Figure 2H**), it remained unclear whether they are available during social behaviors. We therefore performed ASAP5 voltage photometry to monitor BNSTp $V_m$ dynamics during social interaction with female intruders. ASAP5 signals were validated in acute slices and reliably reported depolarizing and hyperpolarizing $V_m$ changes (**Figures 5J-5M**) (38). In freely moving mice, ASAP5 fluorescence revealed an event-locked population-level hyperpolarization around the onset of social contact with the female intruder (**Figures 5N-5O**). This hyperpolarized $V_m$ state may provide a physiological context for $Na_V1.5$-dependent spike initiation during social-cue processing.

We then compared calcium responses before and after *Scn5a* KD. Recordings were performed at 3–8 days and >3 weeks after shRNA virus injection, corresponding to pre-KD and post-KD conditions. Immunostaining at 8 and 12 days after viral injection confirmed residual $Na_V1.5$ expression during the early post-injection period (**Figures 3F** and **S5A**). *Scn5a* KD selectively attenuated responses to female urine, while responses to male and female intruders and male urine were largely preserved (**Figures 6A-6C**). Accordingly, the urine-cue preference estimated from calcium responses was eliminated after *Scn5a* KD (**Figure 6D**). *Scn5a* KD also reduced both the amplitude and the onset slope of calcium signals evoked by female urine (**Figures 6E-6G**), consistent with the elevated AP threshold and delayed AP initiation observed in slice recordings (**Figures 3J-3L**).

Behavior-aligned analyses further showed that calcium responses during female-directed anogenital sniffing were more strongly reduced after *Scn5a* KD than in control recordings, whereas signals during female-directed body investigation and male-directed behaviors showed comparable changes across sessions (**Figures 6H-6J** and **S5B-S5G**). These results suggest that $Na_V1.5$ preferentially supports BNSTp population responses associated with female-directed chemosensory investigation, while responses to male cues or general social contact are less dependent on $Na_V1.5$ under these conditions.

## Discussion

This study identifies $Na_V1.5$ as a state-dependent regulator of BNSTp neuronal excitability during social-cue processing. Its AIS localization and voltage-dependent availability allow it to preferentially support spike initiation under relatively hyperpolarized membrane-potential states. Consistently, *Scn5a* KD depolarized AP threshold, delayed AP initiation, and selectively weakened female-urine-evoked calcium responses in male mice. ASAP5 photometry further revealed a hyperpolarizing state of $Na_V1.5^+$ neurons during social

interaction with female intruders, providing an in vivo context in which $Na_V1.5$ may modulate BNSTp responses to salient social cues (**Figures 5J-5O**).

BNSTp $Na_V1.5^+$ neurons were robustly activated during initial social contact, especially by female intruders and female urine, but were not exclusively tuned to opposite-sex cues. Pup-evoked responses were comparable to female-evoked responses, supporting a broader role of BNSTp $Na_V1.5^+$ neurons in salient social-cue processing related to pup directed behaviors(39) (**Figures 5G-5I**). Mating-aligned analyses further showed stronger engagement during early female investigation than during mating behavior, with weak but detectable activation at ejaculation (**Figures S4A-S4C**). This pattern differs from BNSTp $Aro^+$ neurons, which show strong activation during intromission and ejaculation(9), suggesting that $Na_V1.5^+$ and $Aro^+$ neurons may represent partially overlapping but functionally distinct BNSTp populations. Consistently, *Scn5a* KD reduced both appetitive and consummatory female-directed behaviors, a phenotype distinct from manipulations of $Aro^+$, $Tac1^+$, or $Esr1^+$ BNSTp neurons(5,9,32).

Additional data further refine this interpretation. *Scn5a* was broadly expressed among urine-responsive BNSTp neurons (**Figures S3E-S3I**), and chemogenetic activation of $Na_V1.5^+$ BNSTp neurons did not impose female preference (**Figures S3D**). Thus, $Na_V1.5$ is not selectively enriched in female-cue-responsive neurons and is not sufficient to modulate female preference by artificial excitation alone. Instead, $Na_V1.5$ appears to facilitate female chemosensory processing in a physiological context in which neurons are relatively hyperpolarized. Because sex-specific social behaviors are shaped by internal state, experience, and environmental cues(11,12,35,40,41), future work should test whether $Na_V1.5$ expression or gating is dynamically regulated under these conditions.

Our circuit analyses identify the PMv as a prominent downstream target of BNSTp $Na_V1.5^+$ neurons (**Figure S1E**). PMv-projecting BNSTp neurons were

recruited by intruder and urine stimuli (**Figures S4D-S4G**). Although the PMv is classically associated with male-directed aggression and male-cue-biased coding(6,8), it can also respond to female cues(8,14,42), raising the possibility that PMv-projecting BNSTp neurons contain distinct social-cue-responsive subpopulations. However, because the main photometry and *Scn5a* KD experiments were not projection-specific, we interpret this projection as a socially responsive output pathway that potentially influenced by $Na_V1.5$-dependent excitability rather than a definitive BNSTp-to-PMv mating circuit.

The comparable *Scn5a* expression in male and female BNSTp also raises the question of whether $Na_V1.5$ regulates social-cue processing in females. Our experiments confirmed AIS-localized $Na_V1.5$ expression and broad social stimulus responses in female mice, with particularly strong responses to pups (**Figures S6**). Given the enrichment of $Na_V1.5$ in sexually dimorphic brain regions, it remains to be determined whether $Na_V1.5$ contributes to sex-specific behaviors in males and females.

In conclusion, $Na_V1.5$ fine-tunes BNSTp neuronal excitability during social-cue processing and may increase the gain and temporal precision of responses to salient social stimuli. In male mice, this mechanism contributes to female-cue processing and female-directed social behaviors. Whether $Na_V1.5$-dependent excitability mechanisms contribute to altered social motivation or affective behavior in disease contexts remains an important question for future studies.

## Author Contributions

W.K. performed most experiments and data analysis. H.Z. assisted with behavioral and *in vivo* experiments. L.L. and Y.X. assisted with ASAP5 imaging. S.L. and Q.H. assisted with data analysis. X.Z. managed and bred transgenic mouse lines. L.Y. and Y.T. assisted with behavioral annotation and paradigm

441 design. Y.S. conceived and supervised the study. W.K. and Y.S. wrote the
442 manuscript with input from all authors.

## 443 Acknowledgments

444 This study was supported by the National Natural Science Foundation of China
445 (32130044 and T2241002 to Y.S., 32200953 to W.K., and 32100930 to Q.H.),
446 the STI2030-Major Projects of the Ministry of Science and Technology of China
447 (2021ZD0202500 to Y.S.), and the Science and Technology Commission of
448 Shanghai Municipality Program of Shanghai Academic/Technology Research
449 Leader (21XD1400100 to Y.S.). The funders had no role in study design, data
450 collection and analysis, decision to publish, or manuscript preparation.
451 ChatGPT was used only for language editing and stylistic refinement, and all
452 scientific content was developed, verified, and approved by the authors.

## 453 Financial Disclosures

454 All authors report no biomedical financial interests or potential conflicts of
455 interest.

## 456 Data availability

457 All datasets are available from the corresponding author upon request
458 (Yousheng: yousheng@fudan.edu.cn). The custom-written codes are available
459 at https://github.com/Youshengshu/BNSTp_Nav1.5.

460

461 **Supplement Description:**

462 Figures S1-S6

463

Journal Pre-proof

# References


1. Li Y, Dulac C (2018): Neural coding of sex-specific social information in the mouse brain. *Current Opinion in Neurobiology* 53: 120–130.
2. Chen P, Hong W (2018): Neural Circuit Mechanisms of Social Behavior. *Neuron* 98: 16–30.
3. Bayless DW, Davis CO, Yang R, Wei Y, De Andrade Carvalho VM, Knoedler JR, *et al.* (2023): A neural circuit for male sexual behavior and reward. *Cell* 186: 3862-3881.e28.
4. Lischinsky JE, Yin L, Shi C, Prakash N, Burke J, Shekaran G, *et al.* (2023): Transcriptionally defined amygdala subpopulations play distinct roles in innate social behaviors. *Nat Neurosci* 26: 2131–2146.
5. Yang B, Karigo T, Anderson DJ (2022): Transformations of neural representations in a social behaviour network. *Nature* 608: 741–749.
6. Chen A-X, Yan J-J, Zhang W, Wang L, Yu Z-X, Ding X-J, *et al.* (2020): Specific Hypothalamic Neurons Required for Sensing Conspecific Male Cues Relevant to Inter-male Aggression. *Neuron* 108: 763-774.e6.
7. Ishii KK, Osakada T, Mori H, Miyasaka N, Yoshihara Y, Miyamichi K, Touhara K (2017): A Labeled-Line Neural Circuit for Pheromone-Mediated Sexual Behaviors in Mice. *Neuron* 95: 123-137.e8.
8. Guo Z, Yin L, Diaz V, Dai B, Osakada T, Lischinsky JE, *et al.* (2023): Neural dynamics in the limbic system during male social behaviors. *Neuron* 111: 3288-3306.e4.
9. Bayless DW, Yang T, Mason MM, Susanto AAT, Lobdell A, Shah NM (2019): Limbic Neurons Shape Sex Recognition and Social Behavior in Sexually Naive Males. *Cell* 176: 1190-1205.e20.
10. Li Y, Mathis A, Grewe BF, Osterhout JA, Ahanonu B, Schnitzer MJ, *et al.* (2017): Neuronal Representation of Social Information in the Medial Amygdala of Awake Behaving Mice. *Cell* 171: 1176-1190.e17.
11. McHenry JA, Otis JM, Rossi MA, Robinson JE, Kosyk O, Miller NW, *et al.* (2017): Hormonal gain control of a medial preoptic area social reward circuit. *Nat Neurosci* 20: 449–458.
12. Wei A, Zhao A, Zheng C, Dong N, Cheng X, Duan X, *et al.* (2025): Sexually dimorphic dopaminergic circuits determine sex preference. *Science* 387: eadq7001.
13. Yan R, Wei D, Varshneya A, Shan L, Dai B, Asencio HJ, *et al.* (2024): The multi-stage plasticity in the aggression circuit underlying the winner effect. *Cell* 187: 6785-6803.e18.
14. Mei L, Osakada T, Lin D (2023): Hypothalamic control of innate social behaviors. *Science* 382: 399–404.
15. Osakada T, Ishii KK, Mori H, Eguchi R, Ferrero DM, Yoshihara Y, *et al.* (2018): Sexual rejection via a vomeronasal receptor-triggered limbic circuit. *Nat Commun* 9: 4463.
16. Alsaloum M, Dib-Hajj SD, Page DA, Ruben PC, Krainer AR, Waxman SG (2025): Voltage-gated sodium channels in excitable cells as drug targets. *Nat Rev Drug Discov* 24: 358–378.
17. Abriel H (2007): Roles and regulation of the cardiac sodium channel Nav1.5: Recent insights from experimental studies. *Cardiovascular Research* 76: 381–389.

18. Donahue LM, Coates PW, Lee VH, Ippensen DC, Arze SE, Poduslo SE (2000): The cardiac sodium channel mRNA is expressed in the developing and adult rat and human brain. *Brain Research* 887: 335–343.
19. Hartmann HA, Colom LV, Sutherland ML, Noebels JL (1999): Selective localization of cardiac SCN5A sodium channels in limbic regions of rat brain. *Nat Neurosci* 2: 593–595.
20. Yin L, Hashikawa K, Hashikawa Y, Osakada T, Lischinsky JE, Diaz V, Lin D (2022): VMHvlICckar cells dynamically control female sexual behaviors over the reproductive cycle. *Neuron* 110: 3000-3017.e8.
21. Hu W, Tian C, Li T, Yang M, Hou H, Shu Y (2009): Distinct contributions of Nav1.6 and Nav1.2 in action potential initiation and backpropagation. *Nat Neurosci* 12: 996–1002.
22. Stirling DR, Swain-Bowden MJ, Lucas AM, Carpenter AE, Cimini BA, Goodman A (2021): CellProfiler 4: improvements in speed, utility and usability. *BMC Bioinformatics* 22: 433.
23. Falkner AL, Dollar P, Perona P, Anderson DJ, Lin D (2014): Decoding Ventromedial Hypothalamic Neural Activity during Male Mouse Aggression. *J Neurosci* 34: 5971–5984.
24. Welch JD, Kozareva V, Ferreira A, Vanderburg C, Martin C, Macosko EZ (2019): Single-Cell Multi-omic Integration Compares and Contrasts Features of Brain Cell Identity. *Cell* 177: 1873-1887.e17.
25. Gegenhuber B, Wu MV, Bronstein R, Tollkuhn J (2022): Gene regulation by gonadal hormone receptors underlies brain sex differences. *Nature* 606: 153–159.
26. Giardino WJ, Eban-Rothschild A, Christoffel DJ, Li S-B, Malenka RC, De Lecea L (2018): Parallel circuits from the bed nuclei of stria terminalis to the lateral hypothalamus drive opposing emotional states. *Nat Neurosci* 21: 1084–1095.
27. Jennings JH, Sparta DR, Stamatakis AM, Ung RL, Pleil KE, Kash TL, Stuber GD (2013): Distinct extended amygdala circuits for divergent motivational states. *Nature* 496: 224–228.
28. Li L, Huang Q, Hu J, Ke W, Zhuo Y, He Q, *et al.* (2025): Selective Loss of Scn2a in Ventral Tegmental Area Dopaminergic Neurons Leads to Dopamine System Hypofunction and Autistic-Like Behaviors. *Neuron* 1–18.
29. Li T, Tian C, Scalmani P, Frassoni C, Mantegazza M, Wang Y, *et al.* (2014): Action Potential Initiation in Neocortical Inhibitory Interneurons ((A. Bacci, editor)). *PLoS Biol* 12: e1001944.
30. Savio-Galimberti E, Gollob MH, Darbar D (2012): Voltage-Gated Sodium Channels: Biophysics, Pharmacology, and Related Channelopathies. *Front Pharmacol* 3. https://doi.org/10.3389/fphar.2012.00124
31. Resch JM, Fenselau H, Madara JC, Wu C, Campbell JN, Lyubetskaya A, *et al.* (2017): Aldosterone-Sensing Neurons in the NTS Exhibit State-Dependent Pacemaker Activity and Drive Sodium Appetite via Synergy with Angiotensin II Signaling. *Neuron* 96: 190-206.e7.
32. Shu Y, Hasenstaub A, Duque A, Yu Y, McCormick DA (2006): Modulation of intracortical synaptic potentials by presynaptic somatic membrane potential. *Nature* 441: 761–765.

33. Kirkton RD, Bursac N (2011): Engineering biosynthetic excitable tissues from unexcitable cells for electrophysiological and cell therapy studies. *Nat Commun* 2: 300.
34. Knoedler JR, Inoue S, Bayless DW, Yang T, Tantry A, Davis C, *et al.* (2022): A functional cellular framework for sex and estrous cycle-dependent gene expression and behavior. *Cell* 185: 654-671.e22.
35. Zhou X, Li A, Mi X, Li Y, Ding Z, An M, *et al.* (2023): Hyperexcited limbic neurons represent sexual satiety and reduce mating motivation. *Science* 379: 820–825.
36. Pankevich DE, Baum MJ, Cherry JA (2004): Olfactory Sex Discrimination Persists, Whereas the Preference for Urinary Odorants from Estrous Females Disappears in Male Mice after Vomeronasal Organ Removal. *J Neurosci* 24: 9451–9457.
37. Yao S, Bergan J, Lanjuin A, Dulac C (2017): Oxytocin signaling in the medial amygdala is required for sex discrimination of social cues. *eLife* 6: e31373.
38. Hao YA, Lee S, Roth RH, Natale S, Gomez L, Taxidis J, *et al.* (2024): A fast and responsive voltage indicator with enhanced sensitivity for unitary synaptic events. *Neuron* 112: 3680-3696.e8.
39. Mei L, Wang Y, Wei Q, Xiong Y, O'Neill PT, Yang B, et al. (2026): The neural control of infanticide and parental behaviors in male mice. bioRxiv [Preprint]. 2026 Mar 13:2026.03.12.711470. doi:10.64898/2026.03.12.711470.
40. Wang Y, Song X, Chen X, Zhou Y, Ma J, Zhang F, *et al.* (2025): Integrating reproductive states and social cues in the control of sociosexual behaviors. *Cell* 188: 3530-3549.e24.
41. Nomoto K, Lima SQ (2015): Enhanced Male-Evoked Responses in the Ventromedial Hypothalamus of Sexually Receptive Female Mice. *Current Biology* 25: 589–594.
42. Cavalcante JC, Bittencourt JC, Elias CF (2006): Female odors stimulate CART neurons in the ventral premammillary nucleus of male rats. *Physiology & Behavior* 88: 160–166.

Journal Pre-proof

## Figures and figure legends

**Figure 1. *Scn5a* expresses in a subpopulation of BNST neurons.**

(A) Schematic illustrating the anatomical organization of the BNST and its subregions. Anterior (BNSTa including ov, am and al subdivisions, red) and posterior (BNSTp including pr and if, blue) regions are shown with corresponding bregma coordinates.

(B) Representative images of fluorescence *in situ* hybridization (RNAscope) demonstrating *Scn5a* mRNA expression (green) in BNSTa and BNSTp.

(C) Top, pie plot illustrating the proportion of *Scn5a*$^{+}$ and *Scn5a*$^{-}$ neurons in BNSTa and BNSTp. The inner ring denotes regional distribution of total BNST neurons, and the outer ring indicates the proportion of *Scn5a*$^{+}$ neurons in BNSTp (40.6%) and BNSTa (28.0%). Bottom, the number and proportion of *Scn5a*$^{+}$ neurons across refined subregions from the scRNA-seq dataset.

(D) Coexpression of *Scn5a* with established BNST cell type markers, including *Esr1*, *Esr2*, *Ar*, *Tac1*, *Tac2*, *Cyp19a1 and Slc32a1* (encoding Vgat).

(E) Top, schematic illustration of retrograde labeling of different BNST neurons (targeting PMv, VTA, or PAG, red). Bottom, representative coronal brain section showing retrobeads injection into bilateral PMv (blue, DAPI; red, retrobeads).

(F) Left, representative RNAscope images showing *Scn5a* expression in BNST neurons retrogradely labeled from the PMv. Right, RNAscope signals (*Scn5a*, green) and retrobeads (red).

(G) Representative images showing *Scn5a* expression in BNST neurons retrogradely labeled from VTA and PAG.

(H) Plots of the number of *Scn5a*$^{+}$ and *Scn5a*$^{-}$ cells in neurons from BNST subregions labeled by retrobeads (injected to VTA, PAG, and PMv).

Data are presented as mean ± SEM.

**Figure 2. Nav1.5 accumulates at the AIS and mediates TTX-resistant $Na^+$ currents.**

(A) Representative images showing Nav1.5 immunosignals (green) at the AnkG-labeled AIS (red). Dashed lines indicate the locations of somata.

(B) Representative whole-cell $Na^+$ currents with and without TTX (1μM).

(C) Amplitude distribution of total(n = 38 cells from 2 mice) and TTX-resistant Na+ currents across recorded cells (n = 47 cells from 5 mice).

(D) Example trace of TTX-resistant $Na^+$ currents before and after the bath application of QX-314 (0.5 mM).

(E) Group data of QX-314 (n = 7 cells from 4 mice, paired t-test).

(F) Example traces showing presence (somatic whole-cell recording, top) and absence (somatic nucleated patch recording, bottom) of TTX-resistant $Na^+$ currents.

(G) Example traces of axon bleb recording showing the presence of TTX-resistant $Na^+$ currents (red, activation; gray, steady-state inactivation).

(H) Activation and steady-state inactivation curves of TTX-resistant $Na^+$ currents recorded from axonal blebs. Activation: n = 5 blebs from 4 mice; inactivation: n = 7 blebs from 5 mice.

(I) Bar plots of the half-activation and half-inactivation voltage ($V_{1/2}$) and the corresponding slopes of TTX-resistant $Na^+$ currents.

Data are presented as mean ± SEM. *p < 0.05, **p < 0.01, ***p < 0.001.

**Figure 3. Nav1.5 lowers AP threshold and accelerates AP initiation at hyperpolarized $V_m$.**

(A) Representative confocal images showing *post hoc* avidin staining (green) of a recorded BNSTp neuron and Nav1.5 immunosignals (red) along the AnkG-stained AIS (blue).

(B) Left, quantification of Nav1.5 and AnkG immunosignal intensity along the AIS in $Na_V1.5^+$ (orange, n = 21 cells from 2 mice) and $Na_V1.5^-$ (gray, n = 23

cells from 2 mice) neurons. Right, group data comparing the peak $Na_V1.5$ immunosignal intensity. Wilcoxon rank sum test.

(C) Top, representative voltage responses to step current injections in $Na_V1.5^+$ (orange) and $Na_V1.5^-$ (gray) neurons. Bottom, expanded traces showing the initial APs.

(D) Comparison of AP properties. $Na_V1.5^+$, n = 21 cells from 2 mice; $Na_V1.5^-$, n = 23 cells from 2 mice. Wilcoxon rank sum test and two-sample t-test.

(E) Schematic illustrating injections of viruses carrying *Scn5a* (KD) or scramble shRNA (Ctrl) into the BNSTp, and retrobeads into the PMv.

(F) Example images showing $Na_V1.5$ immunostaining in Ctrl and *Scn5a*-KD mice.

(G) Left, representative traces showing presence and absence of TTX-resistant $Na^+$ currents in Ctrl and KD mice, respectively. Right, amplitude distribution of TTX-resistant $Na^+$ current from neurons in Ctrl and KD group (Ctrl: n = 52 cells from 2 mice, KD: n = 39 cells from 2 mice).

(H) Frequency-current (F-I) curves of Ctrl and *Scn5a*-KD neurons.

(I) Overlay of the first AP waveforms evoked at hyperpolarized $V_m$ (top) and resting $V_m$ (RMP, bottom), as well as their corresponding phase plots in Ctrl and KD neurons.

(J-L) Comparisons of the voltage threshold, peak amplitude, and onset latency of the initial APs evoked at hyperpolarized $V_m$ (Ctrl: n = 38 cells from 4 mice, KD: n = 25 cells from 3 mice) or RMP (Ctrl: n = 11 cells from 4 mice, KD: n = 8 cells from 3 mice) in Ctrl and *Scn5a*-KD neurons. Wilcoxon rank sum test and two-sample t-test.

For box plots, the box represents the interquartile range (IQR), with the line inside indicating the median. The whiskers extend to the smallest and largest values within 1.5 x IQR from the first and the third quartiles (Q1 and Q3). * $p < 0.05$, ** $p < 0.01$, *** $p < 0.001$.

**Figure 4. *Scn5a* KD in BNSTp neurons diminishes sex preference and female-directed behavior, but not sex discrimination.**

(A) Representative heatmaps showing locomotion trajectories of Ctrl and KD male mice in the male/female urine preference test.

(B) Left, number of entries into specific zones in Ctrl and *Scn5a*-KD males. Right, the preference index calculated based on entry frequencies: ($E_{female}$ - $E_{male}$) / ($E_{female}$ + $E_{male}$). Ctrl, n = 11 mice, KD, n = 12 mice. Two-way ANOVA (left) and two-sample t-test (right).

(C) Similar to B, but for comparison of the total time spent investigating male- and female-urine zones. Two-way ANOVA (left) and two-sample t-test (right)

(D) Example traces of the urine habituation-dishabituation test. Note the reduced investigation time across repeated male urine presentations (3 times), and the dishabituation upon first exposure to female urine.

(E) Quantification of the investigation time before and after the transition from the third male-urine presentation to the first female-urine presentation. Ctrl, n = 8 mice; KD, n = 8 mice. Two-way ANOVA.

(F) Representative behavior annotation (anogenital sniffing, investigation, and attempt to mount) during free social interaction with a female intruder.

(G) Locomotion in an open field. Note no significant difference in total distance traveled and total time spent in the center zone. Ctrl, n = 11 mice; KD, n = 12 mice. Two-sample t-test.

(H) Cumulative interaction duration across the testing period for Ctrl and KD males toward male and female intruders. Ctrl, n = 10 mice; KD, n = 9 mice. Two-way ANOVA (comparison of data at 250-300 s).

(I) Left, cumulative probability of the duration of each bout duration with female intruders (Kruskal-Wallis H test). Right, group data comparing the mean duration of each bout of social interaction (Two-way ANOVA).

(J) Bar plots of the number of mounting events. Ctrl, n = 15 mice; KD, n = 14 mice. Mann-Whitney U test.

For box plots, the box represents the interquartile range (IQR), with the line

inside indicating the median. The whiskers extend to the smallest and largest values within 1.5 x IQR from the first and the third quartiles (Q1 and Q3). * $p < 0.05$, ** $p < 0.01$, *** $p < 0.001$.

**Figure 5. $Na_V1.5$-expressing neurons in male BNSTp respond strongly to salient social stimuli and show contact-associated hyperpolarization.**

(A) Experimental paradigm. $Na_V1.5$-cre mice receive bilateral BNSTp virus injections allowing cre-dependent jRGECO1a expression, followed by injections of scramble shRNA viruses (Ctrl) and fiber implantation for longitudinal fiber photometry.

(B) Left, location of fiber implantation from all recorded mice. Right, a representative image showing virus infection and fiber track in the BNSTp.

(C) Top, calcium transients of BNSTp neurons in a Ctrl male mouse associated with first contact with a female intruder in the two recording sessions (pre vs. post), and average trace (n = 8 mice). Bottom, calcium signals associated with first contact with female urine.

(D) An example calcium trace from a Ctrl male during interaction with a female intruder, annotated with different behavioral types, i.e., first contact, anogenital sniffing, investigation, and attempt to mount.

(E) Average traces of calcium responses associated with different behavioral types in D.

(F) Plot of the peak calcium amplitude across the initial 9 bouts of anogenital sniffing.

(G) Average calcium signals in Ctrl males during the first contact with intruders, urine stimuli, pups, and objects.

(H) Quantification of area under the curve (AUC) of calcium signals associated with different stimuli in Ctrl males. One-way ANOVA. Female- and pup-evoked responses were not significantly different across peak response, AUC, or onset slope.

(I) Preference index calculated by AUC of calcium signals. One-sample t-test.
(J) Representative image showing ASAP5 expression in BNSTp neurons.
(K) *In vitro* validation of ASAP5 signals in BNSTp neurons using simultaneous whole-cell recording and high-speed fluorescence imaging (n = 8 cells from 3 mice). Representative membrane potential traces and corresponding ASAP5 fluorescence signals in response to long (500 ms, raw trace) and brief (2 ms, averaged trace) depolarizing current injections. The asterisks indicate individual AP-aligned fluorescence peaks.
(L) Representative membrane-potential responses and corresponding ASAP5 fluorescence signals (averaged) during hyperpolarizing current injections.
(M) ASAP5 fluorescence change across membrane potentials.
(N) Left, a representative coronal image showing ASAP5 expression and the fiber track in BNSTp. Right, *in vivo* ASAP5 fluorescence traces from BNSTp neurons aligned to the first contact with a female intruder (n = 6 mice). Gray traces, individual mice; the blue trace highlights an example.
(O) Averaged ASAP5 response aligned to the first contact, showing an event-locked fluorescence change (corresponding to hyperpolarization of the imaged neurons).

In F, H, M, and O, data are presented as mean ± SEM. In I, the box represents the interquartile range (IQR), with the line inside indicating the median. The whiskers extend to the smallest and largest values within 1.5 x IQR from Q1 and Q3. * $p < 0.05$, ** $p < 0.01$, *** $p < 0.001$.

**Figure 6. *Scn5a* knockdown selectively attenuates female-urine-evoked BNSTp population responses.**
(A) Experimental paradigm. $Na_V1.5$-cre mice receive bilateral BNSTp virus injections allowing cre-dependent jRGECO1a expression, followed by injections of shRNA viruses (KD) and fiber implantation.

(B) Representative calcium traces in Na$_V$1.5-cre male mice during free investigation of female urine from pre- and post-KD sessions.

(C) Average calcium signals associated with the first contact with intruders or urine stimuli during pre- and post-KD sessions.

(D) Group data showing the preference indexes based on the peak amplitude, i.e., $(Peak_{female}-Peak_{male})/(Peak_{female}+Peak_{male})$, or AUC of calcium responses to urine across pre- and post-KD sessions. Pre-KD, n = 6 mice; post-KD, n = 5 mice. One-sample t-test.

(E) Average calcium signals aligned to the maximal onset slope.

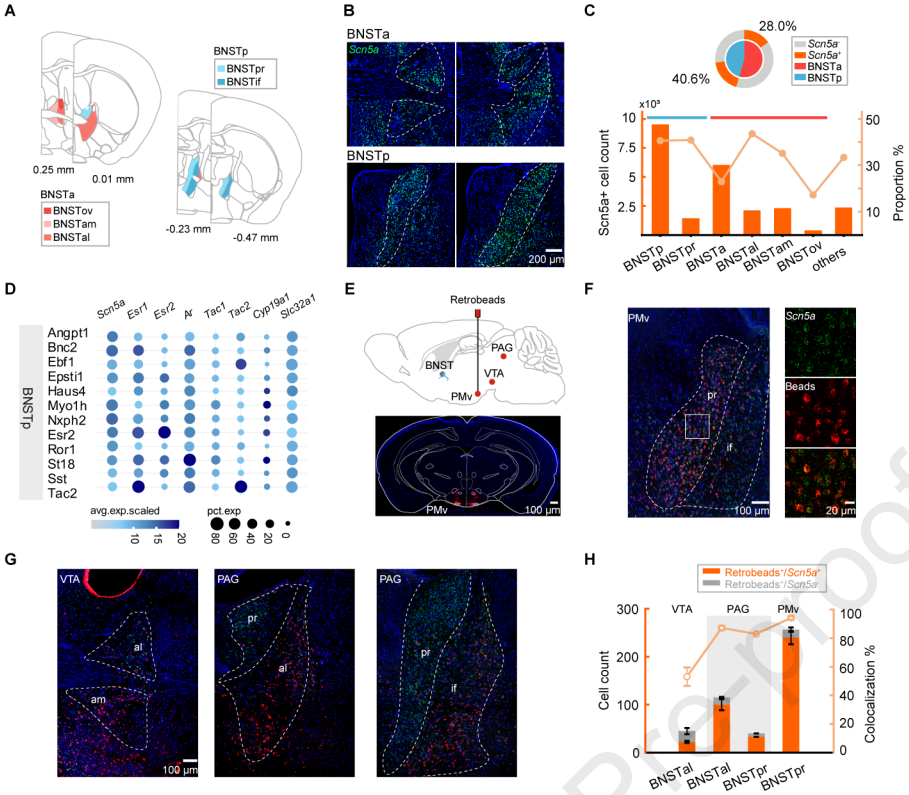
(F-G) Comparison of the amplitude (F) and maximal onset slope (G) of calcium responses to female urine before and after *Scn5a* KD. Pre-KD, n = 6 mice; post-KD, n = 6 mice for intruders, n = 5 mice for urine stimuli. Wilcoxon rank sum test and two-sample t-test.

(H) Heatmaps of calcium responses during anogenital sniffing in pre- and post-sessions in Ctrl and KD male mice.

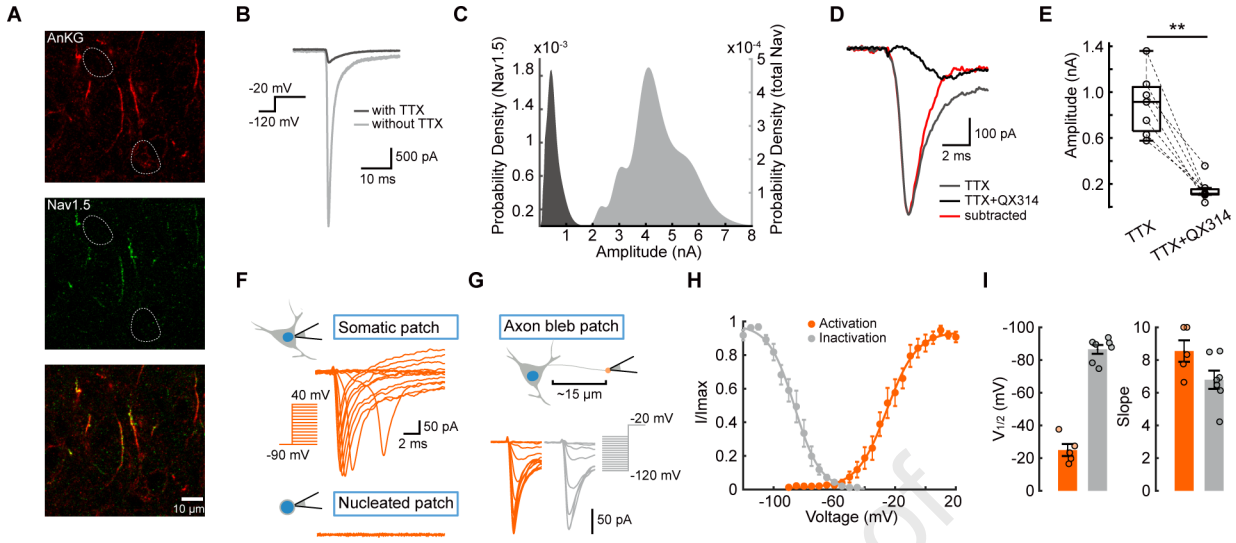
(I) Average calcium signals associated with different behaviors during social interaction with female intruders (anogenital sniffing, investigation, and mounting) in pre- and post-KD sessions.

(J) Group data of peak calcium signals associated with anogenital sniffing. Pre-Ctrl, n = 4 mice; post-Ctrl, n = 3 mice. Pre-KD, n = 5 mice; post-KD, n = 5 mice. Kruskal-Wallis test. The violin plots display the kernel density estimation of the data, with white dots indicating the median, the thick line representing the interquartile range, and the thin whiskers extending to the smallest and largest values within 1.5 x IQR. * $p < 0.05$, ** $p < 0.01$, *** $p < 0.001$.

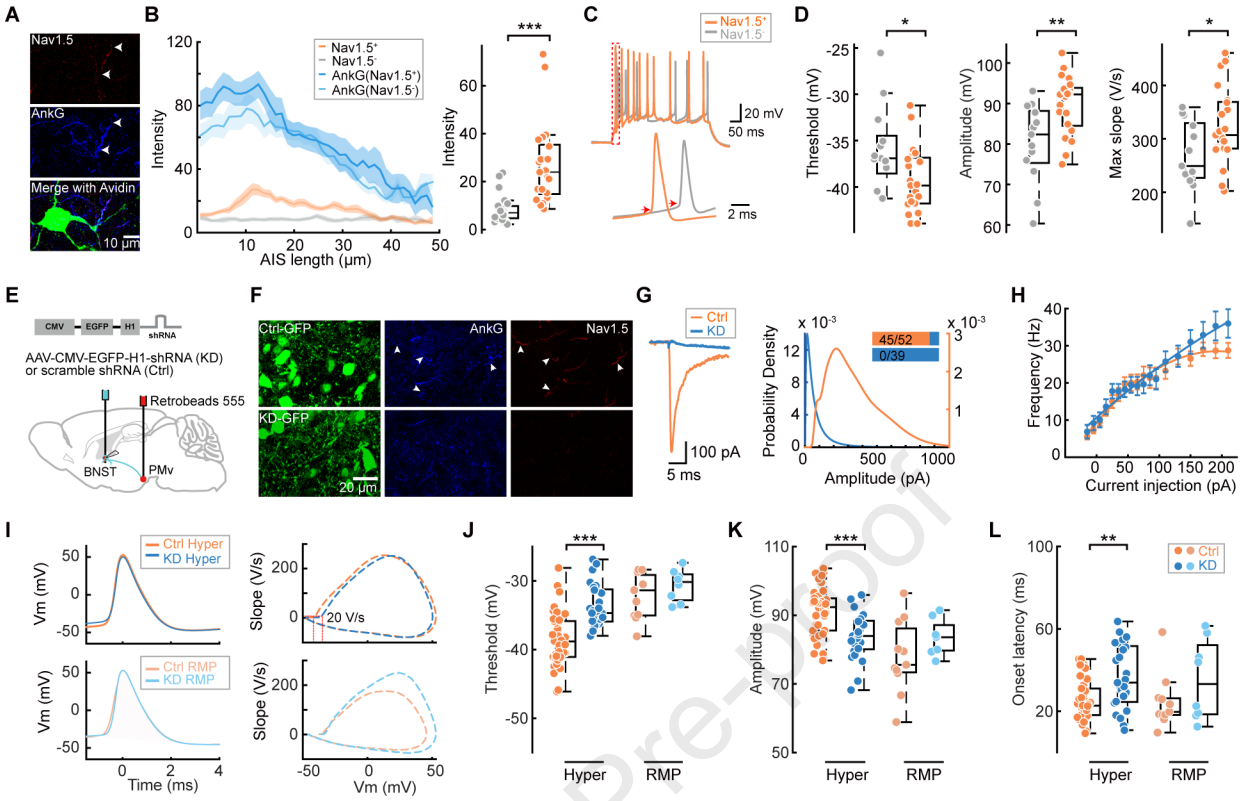
Journal Pre-proof



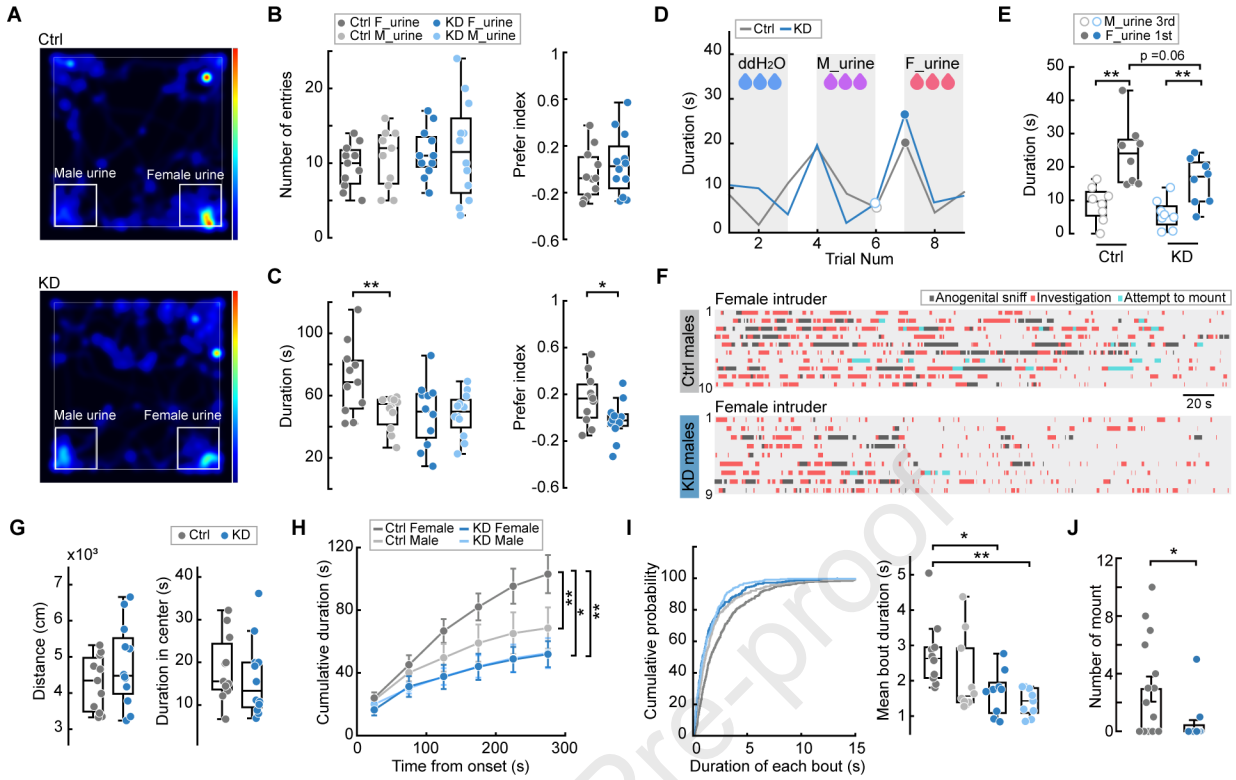

Journal Pre-proof



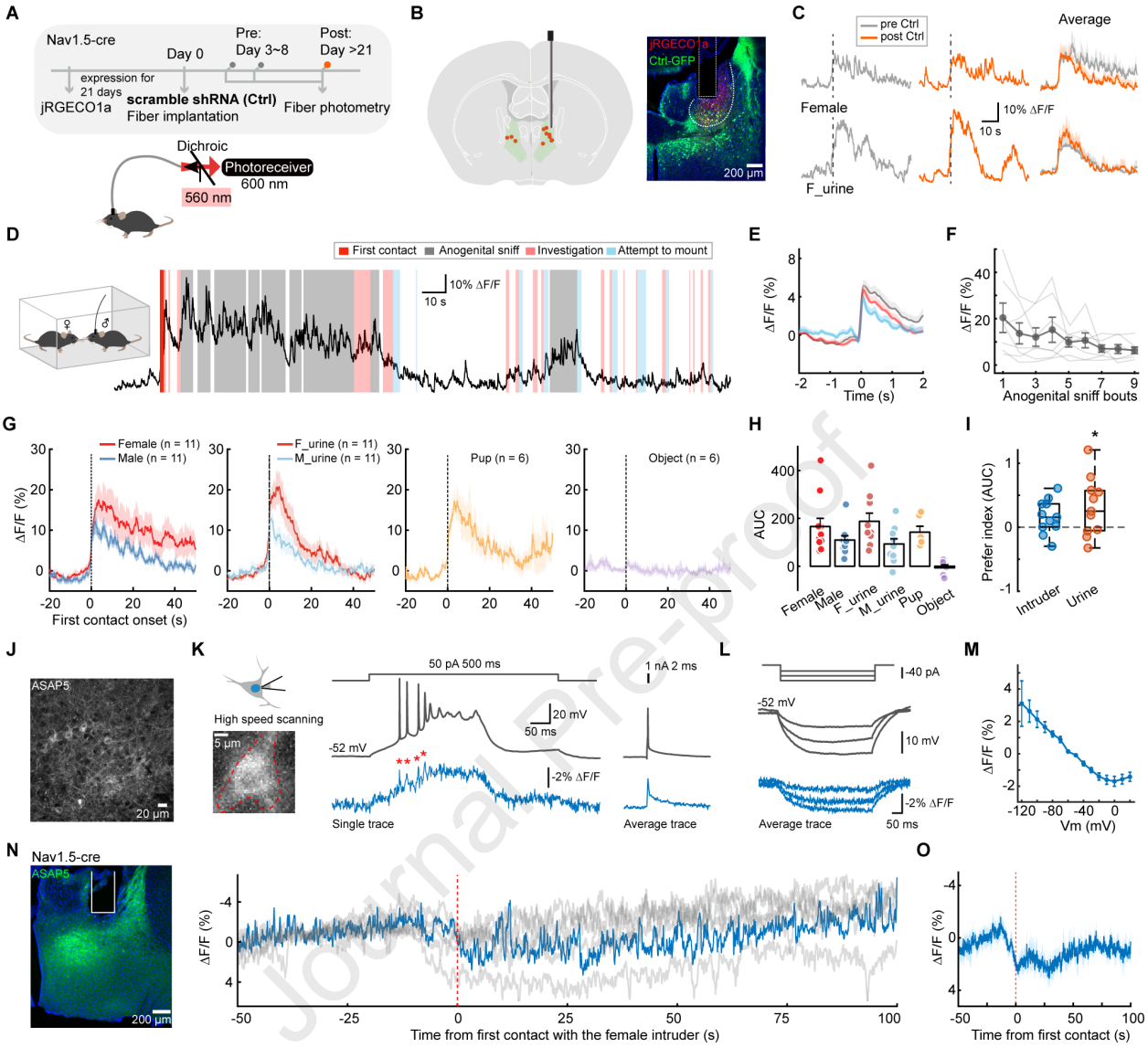

Journal Pre-proof



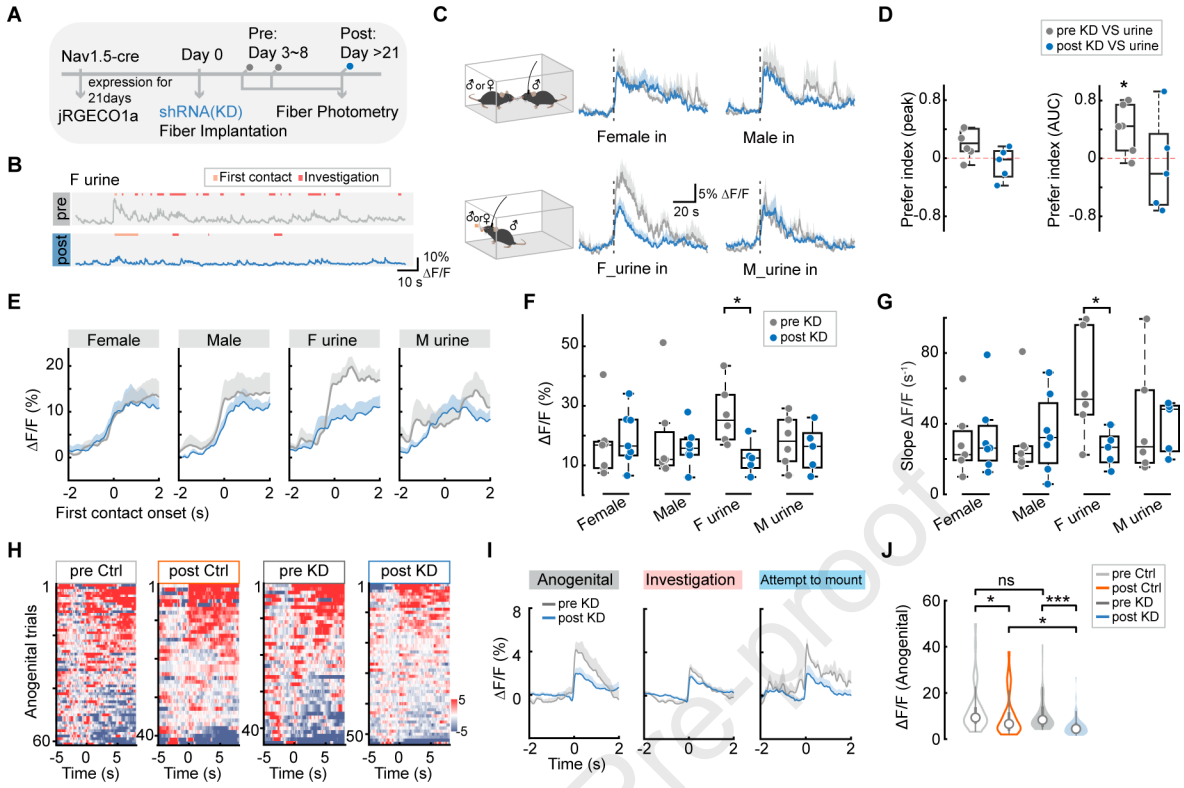

Journal Pre-proof




Journal Pre-proof




Journal Pre-proof




Journal Pre-proof